metals

MDPI

Article

Microstructural Transformations in Solid-State Annealed Al/Ag/Al Diffusion Couples Examined via High-Voltage Electron Microscopy (HVEM)

Minho Oh * and Masanori Kajihara

Department of Materials Science and Engineering, Tokyo Institute of Technology, S8-18, 2-12-1 Ookayama, Meguro-Ku, Tokyo 152-8552, Japan; kajihara@mac.titech.ac.jp
* Correspondence: o.m.aa@m.titech.ac.jp

Abstract: This study focuses on the practical relevance of the Al-Ag bonding interface in electronic device fabrication, particularly in wire bonding, which is crucial for enhancing component reliability and performance. Experiments involved Al/Ag/Al diffusion couples, annealed at 703 K, revealing two stable intermediate phases, μ and δ. Characterizing the intermediate phases' compositions and concentration profiles exposed a vital transition at the δ-Al interface. We used high-voltage electron microscopy (HVEM) to examine crystal structure evolution, identifying a (hexagonal close-packed) hcp structure in the intermediate phase between δ and Al, matching the δ phase. Notably, a substantial microstructural transformation occurred within the Ag-Al diffusion couple, as nano-sized precipitates transitioned from spherical to plate-like, along specific {111} planes, reflecting the evolution from off-stoichiometric, disordered phases to ordered ones. Mapping the concentrations of intermediate phases on the Al-Ag phase diagram revealed shifted and narrower solubility ranges compared to the calculations. This study provides insight into the crystal structure and microstructure changes during diffusion in Al/Ag/Al diffusion couples, holding implications for electronic device fabrication. Understanding intermediate phase behavior and evolution is vital in this context, potentially influencing materials development and process optimization in the electronic components industry, and thus, enhancing device performance and reliability.

Keywords: Ag-Al system; intermediate phase; HVEM; Ag_2Al; metastable phase; EPMA

check for updates

Citation: Oh, M.; Kajihara, M. Microstructural Transformations in Solid-State Annealed Al/Ag/Al Diffusion Couples Examined via High-Voltage Electron Microscopy (HVEM). *Metals* **2023**, *13*, 1780. https://doi.org/10.3390/met13101780

Academic Editor: Jiri Svoboda

Received: 23 September 2023
Revised: 18 October 2023
Accepted: 19 October 2023
Published: 20 October 2023

Copyright: © 2023 by the authors. Licensee MDPI, Basel, Switzerland. This article is an open access article distributed under the terms and conditions of the Creative Commons Attribution (CC BY) license (https://creativecommons.org/licenses/by/4.0/).

1. Introduction

The investigation of the Ag-Al bonding interface holds substantial significance within materials science and engineering, driven by a myriad of compelling rationales: The profound relevance of comprehending the intricacies of the Ag-Al bonding interface becomes conspicuous in the context of electronic device manufacturing [1,2]. Silver, lauded for its superior electrical conductivity, is ubiquitously employed in electronic devices [3]. Conversely, aluminum often serves as the substrate material. An exhaustive grasp of the Ag-Al interface is indispensable for ensuring the efficacy and dependability of electronic connections. In electronic packaging and interconnections, the compatibility of dissimilar materials emerges as a paramount concern. Delving into the intricacies of the Ag-Al bonding interface facilitates the determination of whether these materials can coexist without inauspicious repercussions, such as corrosion or mechanical failures [1]. This discernment assumes critical importance in the design of electronic components with extended longevity and reliability. Exploration into the formation of intermetallic compounds at the Ag-Al interface furnishes invaluable insights into the intricate reactions and transformations that unfold upon the convergence of these metallic entities. These intermetallic compounds can exhibit unique properties, exerting a discernible influence on the overarching performance of electronic devices. Efficient thermal management constitutes a pivotal facet of electronic device design. Attaining a comprehensive understanding of the behavior of the Ag-Al

interface under elevated temperatures is imperative for forecasting and regulating heat dissipation, a parameter with profound ramifications for device performance and longevity.

Diffusion bonding techniques involving dissimilar metals find extensive applications across various industries. The Ag-Al system has emerged as a promising candidate for interconnections between electronic devices and substrates, alongside the well-studied Au-Al and Cu-Al systems [4,5]. Isothermal annealing of diffusion couples composed of dissimilar metals at suitable temperatures leads to the formation of stable compounds as interfacial layers driven by reactive diffusion processes [6,7]. Previous studies have experimentally examined the growth behavior of intermetallic compounds resulting from reactive diffusion in the binary Au-Al and Cu-Al systems [4,5].

In a previous study [5], sandwich diffusion couples were meticulously prepared using a diffusion bonding technique and annealed at solid-state temperatures. In Au/Al diffusion couples, the interface exhibited the presence of three distinct compound layers, Au_8Al_3, AuAl, and $AuAl_2$, even though five stable intermetallic compounds exist at the experimental temperatures. Of note, Au_8Al_3 was predominantly formed in the initial stages and was gradually replaced by AuAl and $AuAl_2$ in the later stages. The identification of a transition in the rate-controlling process for intermetallic layer growth occurred at specific temperatures, and the volume fraction of each compound exhibited variation with annealing time and temperature. In contrast, the formation of all five intermetallic compounds was observed in Cu/Al diffusion couples, and their growth behavior and diffusion kinetics were thoroughly investigated through experimental approaches [4].

Turning our attention to the binary Ag-Al system, the phase diagram indicates the presence of two stable intermediate phases, μ and δ, at temperatures below 723 K [8,9]. Earlier work by [10] using electron microscopy in Ag/Al thin film diffusion couples annealed at 473 K exclusively identified the Ag_2Al phase between the Ag and Al thin films, characterized by elongated crystals aligned along the diffusion direction. Subsequent research by Roy and Sen [11] at 523 K for 1 h, employing electron micrograph and selected-area diffraction (SAD) patterns, corroborated the presence of Ag_2Al precipitates, a conclusion further affirmed by XRD analysis. Schleiwies and Schmitz [12] discerned grain boundary diffusion in Al/Ag thin films through tomographic atom probe analysis, revealing that rapid grain boundary transport of Al into the Ag layer dominated the initial reaction steps. In later stages, a dense layer of metastable $Al_{67}Ag_{33}$ alloy formed, and the final product Ag_2Al precipitated.

Additionally, several investigations have sought to elucidate the crystal structure and ordering of metastable γ′-Ag_2Al and equilibrated γ-Ag_2Al precipitates within Al-rich Ag-Al alloys (Howe et al., 1985; Moore & Howe, 2000; Pang et al., 2012; Zhang et al., 2019) [13–16]. These studies have consistently reported hcp structures for both γ′ and γ precipitates, with a stoichiometric ratio of Ag_2Al [17]. The binary Ag-Al alloy system is a straightforward example of a phase transformation entailing a shift in crystal structure from face-centered cubic (fcc) to hcp [7,18]. Neumann [19] examined the crystal structure of hcp Ag_2Al using X-ray scattering data from a single-crystal Ag-33.2 at.% Al alloy, revealing substantial compositional short-range order (SRO) within the basal plane of hcp. Howe et al. [15] proposed an alternative structure characterized by alternating layers with 100 at.% Ag in one plane and 33 at.% Ag in the next, based on their study of plate-shaped hcp γ′ precipitates. Through simulation, Zarkevich et al. [7] investigated off-stoichiometric disorder in metastable Ag_2Al γ′ nano-precipitates within an fcc Al matrix.

In addition to elucidating the crystal structure and ordering of intermediate phases, our study holds paramount importance in advancing materials science and metallurgy, particularly in the context of electronic device fabrication. Investigating intermediate phases, such as metastable γ′-Ag_2Al and equilibrated γ-Ag_2Al precipitates within Al-rich Ag-Al alloys, is crucial for several reasons. Intermediate phases often possess unique properties that can significantly impact the overall performance of materials. By understanding the growth behavior and characteristics of these phases, we can harness their properties to improve the performance of electronic devices. Insights into intermediate phases provide

valuable information for materials development. These phases can be engineered and tailored to meet specific requirements, creating advanced materials with enhanced electronic properties. Understanding the growth behavior of intermediate phases enables us to optimize manufacturing and fabrication processes. This knowledge can lead to more efficient and cost-effective production methods for electronic components. Intermediate phases can influence the reliability and durability of electronic devices. Studying their behavior allows us to design devices with improved longevity and stability. Investigating intermediate phases contributes to our fundamental understanding of materials and phase transformations. This knowledge not only aids in practical applications but also enriches our comprehension of the underlying principles of materials science.

In the present study, we experimentally investigate the growth behavior of intermediate phases within the binary Ag-Al system by annealing Ag-Al diffusion couples at 703 K. The formation of intermediate layers through precipitates is observed using various advanced techniques, shedding light on this critical aspect of materials science and metallurgy.

2. Materials and Methods

2.1. Preparation of Diffusion Couples and Equilibrated Alloy Specimens

Polycrystalline pure Al plate specimens, measuring $14 \times 5 \times 1.2$ mm^3 and possessing a purity level of 99.99%, underwent mechanical grinding using #600-2000 emery papers. One of the polished surfaces received additional mechanical polishing using #4000 emery paper and was subsequently finished with alumina particles of 1 μm diameter. The Al plate specimen was promptly immersed in ethanol following this surface treatment. Polycrystalline pure Ag sheet specimens, measuring $20 \times 7 \times 0.4$ mm^3, were obtained from a commercial pure Ag sheet with a thickness of 0.4 mm and a purity of 99.99%. Each Ag sheet specimen underwent mechanical grinding and polishing, utilizing alumina particles with a diameter of 1 μm. These Ag sheet specimens were then sandwiched between two prepared Al plate specimens in ethanol, employing a technique previously documented [20]. Each resulting sandwich diffusion couple was thoroughly dried and subsequently subjected to isothermal heat treatment for diffusion bonding within an evacuated silica tube, maintained at 703 K for 24 h, followed by air cooling. The diffusion couples were individually encapsulated within evacuated silica capsules and subjected to isothermal annealing at the same temperature for varying durations, up to 189 h, followed by water quenching without capsule rupture. A binary Ag-Al alloy, containing 25.6 at.% of Ag, was fabricated as a button ingot through Ar arc melting of pure Al and Ag, each boasting a purity level of 99.99% [21]. This alloy specimen was sectioned and subsequently subjected to isothermal annealing within an evacuated silica capsule, sustained at 703 K for 641 h, with subsequent water quenching without capsule damage.

2.2. Observation and Identification of Phases at the Interface

Cross-sections of the annealed diffusion couples were meticulously prepared by mechanical polishing using #1500-4000 emery papers and alumina particles measuring 0.05 μm in diameter. Final surface finishing was accomplished using colloidal silica [22,23]. The microstructure of these cross-sections was examined using a differential interference contrast optical microscope (DICOM). Concentration profiles across the intermediate layers between Ag and Al were quantified via electron probe microanalysis (EPMA). For the equilibrated Ag-Al alloy, the specimen underwent the same polishing techniques described above. Cross-sectional microstructure observations were conducted using back-scattered electron imaging (BEI) via scanning electron microscopy (SEM). To ascertain the crystal structure of the intermediate phases in the Ag-Al diffusion couple, a Hitachi H1250S high-voltage electron microscope (HVEM) [24] was employed, operating at 1020 kV. The HVEM presented distinct advantages, particularly its ability to tilt relatively thick specimens and facilitate wide-range observations. The de Broglie wavelength was calculated to be 0.86×10^{-12} m at 1020 kV, with a camera length of 1.39 m [25]. Thin foiled specimens for HVEM examination

were predominantly prepared from annealed diffusion couples through mechanical and electrolytic polishing. The diffusion couples, comprising intermediate layers approximately 120 µm thick, were mechanically thinned to approximately 40 µm thickness for thin foil preparation perpendicular to the interface direction. Subsequently, the thin foils underwent electrochemical polishing utilizing perchloric acid at 12 V and around 253 K. In cases where the phase was unidentified, specimens were prepared using the H-bar technique via a focused ion beam (FIB) [26]. This technique facilitated the precise localization of each intermediate layer within the diffusion couple, albeit within a limited observable area. X-ray diffraction (XRD) analysis was conducted using a Rigaku Smartlab instrument to determine the crystal structure [6] of the equilibrated Ag-Al alloy. The X-ray source wavelength employed in our XRD analysis was Cu Kα radiation, with a wavelength of 1.5406 Å. We used a standard Bragg-Brentano geometry for our XRD measurements. In this configuration, the incident X-ray beam strikes the sample at a specific angle (θ) and is then diffracted at the same angle (2θ) by the crystal lattice planes within the sample. The detector records the intensity of the diffracted X-rays at various angles to produce the diffraction pattern. We utilized a crystal monochromator to select the Cu Kα wavelength to ensure monochromatic X-ray radiation. This monochromator narrows down the wavelength range for precise diffraction measurements, enhancing the accuracy of our analysis [6].

3. Results

3.1. Microstructure and Compound Growth at the Interface

A representative DICOM photograph of the cross-section of the annealed diffusion couple is depicted in Figure 1a. Specifically, Figure 1a indicates the cross-section of the diffusion couple subjected to annealing at 703 K for 30 h. In this representation, the left region corresponds to the Ag component, while the right region signifies the Al component. Notably, discernible intermediate layers are observed between the Ag and Al constituents. To characterize each of these intermediate layers, concentration profiles across the intermediate regions, normal to the initial interface, were meticulously measured using EPMA, as depicted in Figure 1b. Figure 1b elucidates the concentration profile for the diffusion couple annealed at 703 K for 48 h. In this representation, the ordinate denotes the mole fraction y_i of component i (where i = Ag and Al), while the abscissa represents the distance x. Three intermediate layers exhibiting discontinuous chemical compositions are distinctly discerned between Ag and Al.

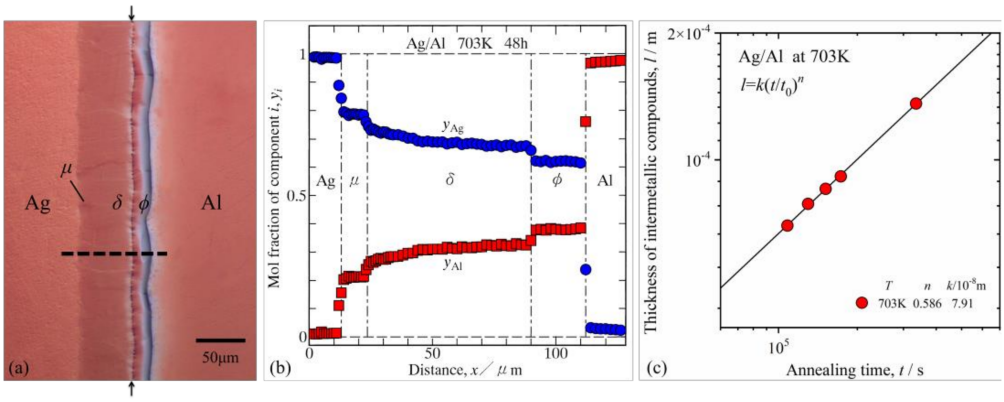


Figure 1. (**a**) Cross-sectional DICOM photograph of Al/Ag/Al diffusion couple annealed at T = 703 K and t = 30 h. (**b**) Concentration profile of Ag and Al across the intermediate layers for the diffusion couple annealed at T = 703 K for t = 48 h. (**c**) The total thickness of the intermetallic layer l versus the annealing time t shown as red circles for T = 703 K. Solid line indicates the calculation from Equation (2).

However, by the binary Ag-Al phase diagram [8], only two stable intermediate phases, referred to as µ and δ, are expected to exist between Ag and Al. A comparison of the composition range observed via the EPMA results and the phase diagram establishes that

the intermediate phase on the Ag-rich side corresponds to the μ phase. In contrast, the middle phase among the three intermediates is identified as the δ phase. The intermediate phase on the Al-rich side aligns with an unknown phase, which we define as ϕ, unaccounted for in the binary Ag-Al phase diagrams [7,8,14,27].

The total thickness l of the intermetallic layer was quantitatively evaluated from DICOM photographs akin to Figure 1a, employing the equation:

$$l = A/w \tag{1}$$

Here, w signifies the total length parallel to the initial Ag/Al interface, and A represents the total area of the intermetallic layer on the cross-section. The results of this analysis are presented as red circles in Figure 1c. To determine the average thickness, we adopted an approach involving calculating the intermetallic compound's area within the cross-section of each diffusion zone sample. Subsequently, we divided this area by the horizontal length w. This method provides us with more dependable average thickness data compared to the conventional technique of repeatedly measuring lengths at various positions. However, it is worth noting that this approach does not incorporate error bars since it does not entail the repetitive collection of data points. In this figure, the ordinate portrays the logarithms of l, while the abscissa corresponds to the logarithms of t, signifying the annealing time. Evidently, l exhibits a monotonous increase with rising annealing time t. Furthermore, the plotted points align well along a linear trajectory. Consequently, l is aptly described as a power function of t, expressed as follows [28–30]:

$$l = k(t/t_0)^n \tag{2}$$

Here, t_0 denotes the unit time, which is 1 s, adopted to render the argument t/t_0 dimensionless. The coefficient k shares dimensions with the thickness l, while the exponent n remains dimensionless. Employing the least-squares method, k and n were computed from the data points, as indicated by the dashed line in Figure 1c. Notably, the exponent n in the power function slightly exceeds 0.5. In cases where the growth of the intermediate layer is governed primarily by volume diffusion, n equals 0.5. Consequently, inserting "$n = 0.5$" into Equation (2) yields an alternate expression of a parabolic relationship [31–33]. However, when interface reactions predominantly influence layer growth, n assumes a value of 1 [34]. Hence, the results suggest that volume diffusion predominantly dictates layer growth, with interface reactions partially contributing to the rate-controlling process. The mixed-rate controlling process is observed in the growth of the intermetallic compounds (IMCs), where both volume diffusion and interface reactions jointly govern the growth rate [35–37]. This phenomenon is commonly encountered in heterogeneous interfaces, particularly at the boundary between two distinct phases. In such cases, the overall reaction rate is constrained by the slower of the two processes, namely, volume diffusion and interface reactions. Volume diffusion, a process reliant on the concentration gradient of reactants within the material, operates simultaneously with interface reactions hinge on the surface area of contact between the phases involved. Consequently, the mixed-rate controlling process of IMC growth emerges as a complex interplay during the formation of IMCs between two metal substrates.

Within this intricate process, IMC growth is concurrently influenced by the rate of atom diffusion through the bulk of the metal and the rate at which atoms are delivered to the interface shared by the two metals [38]. Critical determinants of this mixed-rate controlling process include different materials that possess unique atomic structures and properties that profoundly impact the rate of atomic diffusion and the kinetics of interface reactions [39]. Some materials may readily engage in chemical reactions at the interface, while others may exhibit slower reaction kinetics but faster atomic diffusion rates. The thermodynamic driving forces governing volume diffusion and interface reactions are contingent on the local composition and the stability of involved phases. Regions near compositional equilibrium may favor interface reactions, while regions with compositional

deviations may elevate the prominence of volume diffusion. The presence of defects, grain boundaries, and other microstructural features can significantly affect the rate-controlling process. These structural attributes can serve as preferential sites for interface reactions or impede atomic mobility, thereby promoting volume diffusion.

To elucidate the enigmatic phase situated between the δ phase and the Al matrix within the context of the diffusion couple experiment, an Al-25.6Ag alloy was meticulously prepared through arc melting. Figure 2a offers a representative micrograph, utilizing BEI, capturing the cross-section of the Al-25.6Ag alloy following annealing at 703 K for 641 h. Within this micrograph, discernible bright coarse grains are observed, randomly distributed, and interconnected within a dark matrix. To ascertain the nature of equilibrated phases within this alloy, XRD analysis was conducted on the Al-25.6Ag alloy, as illustrated in Figure 2b. The XRD pattern of the Al-25.6Ag alloy unequivocally confirms the presence of the stable Ag_2Al phase and the coexistence of the Al matrix. The identity of the third phase within the equilibrated Al-25.6Ag alloy remains elusive.

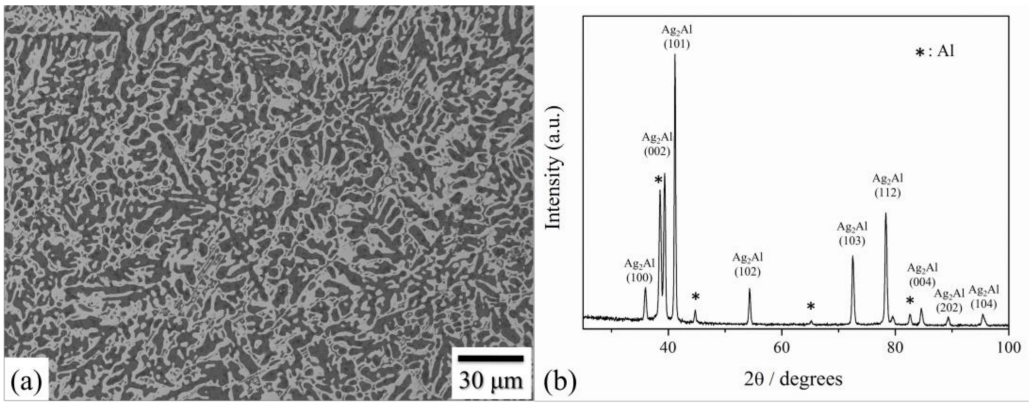


Figure 2. (**a**) Back-scattered electron image and (**b**) X-ray diffraction result of cross-section for Al-25.6Ag alloy annealed at 703 K for 641 h.

3.2. Direct Observation of the Ag/Al Diffusion Couple Using HVEM

For the direct observation of the Ag/Al diffusion couple, specimen preparation was meticulously conducted across three distinct regions corresponding to the Ag-Al intermediate phases within the diffusion couple subjected to annealing at 703 K. In Figure 1a, the continuous line within the intermediate phase, marked by arrows, represents the initial interface. Specimens were separately prepared at various distances from this interface, facilitating the characterization of each area, including the δ phase, the unidentified phase, and the Al side adjacent to the interface between the intermediate phase and the Al matrix. This sequential approach enabled the identification of microstructural changes during the growth of the intermediate phase within the diffusion couple. To ensure precise specimen preparation from the designated location within the diffusion couple, the H-bar technique involving a FIB was employed.

3.2.1. δ Phase

Figure 3 showcases the microstructures and diffraction patterns of the δ phase in the diffusion couple that underwent annealing at 703 K for 48 h. As evident in Figure 3a,b, the δ phase exhibits plate-like structures comprising refined grains within the structure. Diffraction patterns of the hcp structure in the [031] and [011] zones were obtained from the δ phase within the Ag/Al diffusion couple, achieved through sample preparation involving mechanical and electrolytic polishing. Due to small grains within the δ phase, diffraction spots often result from double diffraction, as illustrated in Figure 3b. Consequently, the faint extra spots are displaced from the main pattern of the [011] zone by reflection vectors associated with the small grains within the structure. The hcp structure was unequivocally identified within the δ phase, as indicated by the indices in Figure 3.

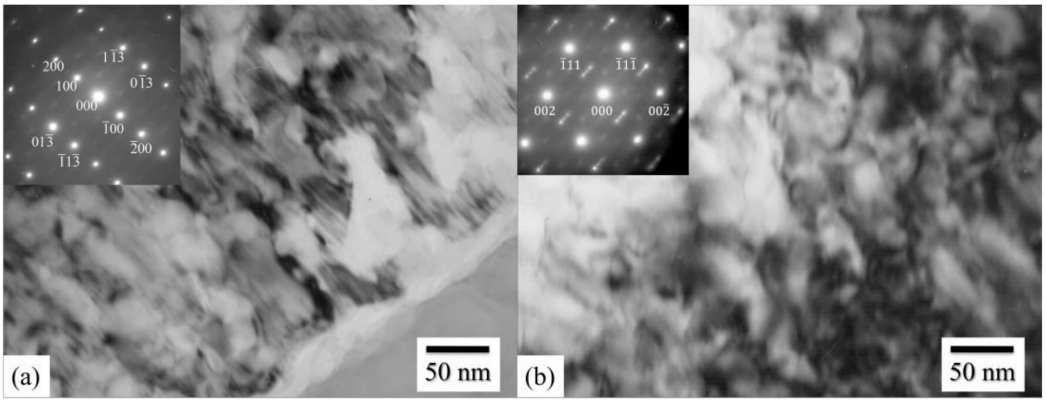


Figure 3. (**a**) Bright-field micrograph and diffraction pattern of a [031] zone. (**b**) Bright-field micrograph and diffraction pattern of a [011] zone taken in δ phase of the Ag/Al diffusion couple annealed at 703 K for 48 h.

3.2.2. Intermediate Phase between δ Phase and Al Matrix

Figure 4 presents the microstructure and diffraction patterns near the initial Ag/Al interface within the diffusion couple annealed at 703 K for 70 h. This figure provides a representative micrograph of the intermediate phase between the δ phase and the Al matrix. As depicted, this phase is characterized by hcp lamellar structures. The diffraction patterns in the [100] zone exhibit streaking between diffraction spots within this intermediate phase. The streaking is observed to run perpendicular to the stacking directions of the lamellar structure. Various factors, such as stacking faults, platelets, thin ordered phases, and thin precipitates, which maintain coherence with the matrix, can contribute to the observed diffused streaking in the diffraction patterns [40]. Thin layers of the lamellar structure, exhibiting streaking between diffraction spots, are presented from a different zone axis in Figure 4b, where the diffuse streaking is superimposed with other diffraction spots. The intensity of the streaking serves as a measure of stacking disorder, indicating changes in the ordering of the plate-like lamellar phase during its growth. Similar diffraction patterns have been reported by Jomni et al. [41] for ultrathin Au/Co multilayers with thicknesses of approximately 1–2 nm. These patterns bear resemblance to Figure 4b. Notably, Co and Au possess distinct crystal structures, specifically hcp and fcc, respectively, yet the global microstructure resembles the lamellar phase within the matrix.

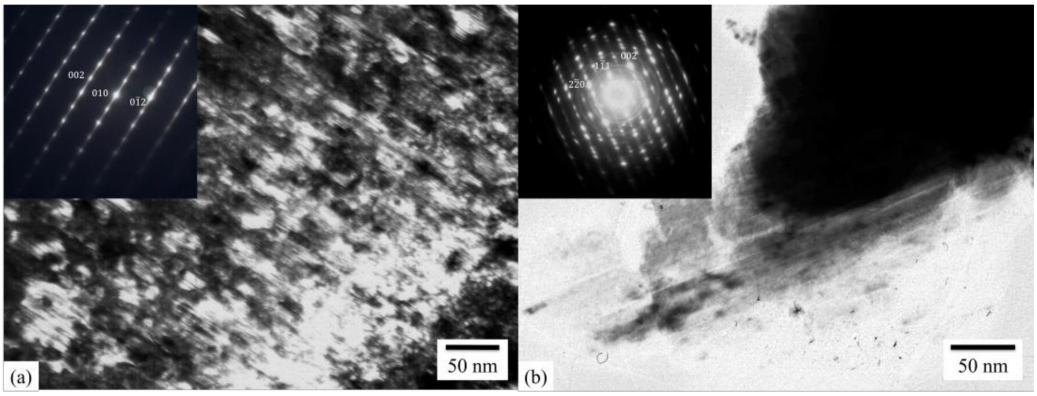


Figure 4. (**a**) Bright-field image showing the microstructure of hcp lamellar phase of a [100] zone. (**b**) Bright-field image showing the microstructure of hcp lamellar phase in fcc matrix with a typical diffraction pattern of thin multilayers. Specimen was prepared in the intermediate phase between δ phase and Al matrix the diffusion couple annealed at 703 K for 70 h.

3.2.3. Intermediate Phases in the Al Side within 40 µm from the Initial Ag/Al Interface

Observations of plate-like precipitates on the Al side, adjacent to the interface between the newly identified intermediate phase and Al within the diffusion couple, are presented in Figure 5. The presence of diffraction patterns with streaking indicates the formation of plate-like hcp phases along the <111> planes within the Al matrix. Notably, the initial spherical nano-sized Guinier–Preston (G-P) zones [42], presumed to be spherical particles within the Al matrix, transform a plate-like shape, growing along specific <111> planes during the diffusion process. This evolution involves the change from spherical G-P zones to faceted plate-like structures along the <111> planes as the precipitates grow [43,44].

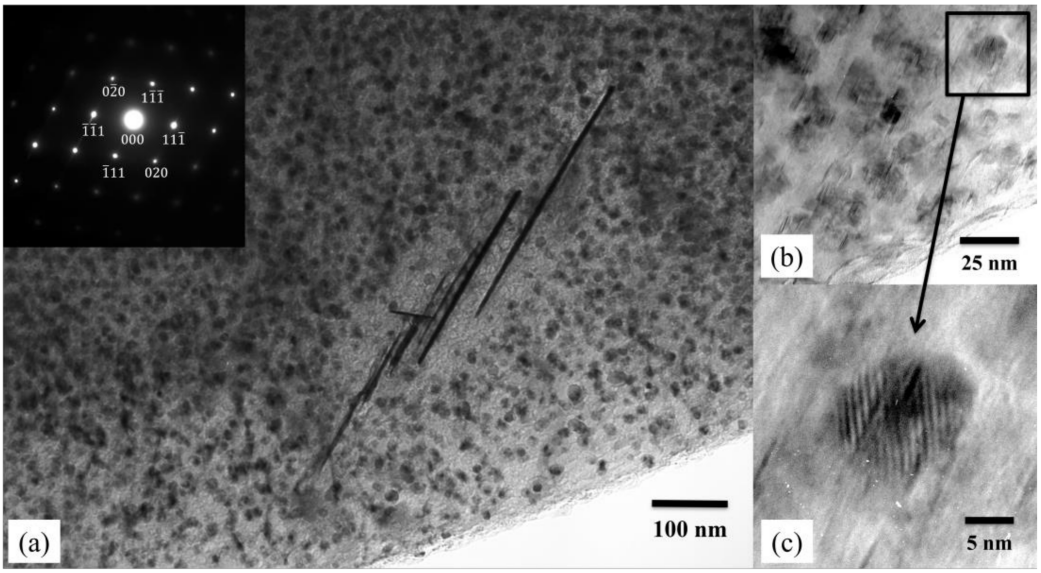


Figure 5. (**a**) Bright-field images showing the microstructure of plate-like γ precipitate in Al matrix observed in Al-rich side of the diffusion couple annealed at 703 K for 70 h and the diffraction pattern of a fcc [011] zone. (**b**) Bright-field image showing the microstructure of plate-like γ precipitates viewed along <110> in Al-rich side of the diffusion couple annealed at 703 K for 189 h. (**c**) An enlarged view of the plate-like γ precipitates embedded within the Al matrix by magnified image of plate-like γ precipitates with Moire-fringes in Al matrix, indicating complex structural interactions within the microstructure.

Figure 5 provides insights into the microstructures of these plate-like intermediate phases, revealing their existence within the Al matrix alongside various Moire fringes. In this context, the incident beam is directed along the <110> direction of Al, with two <111> planes among four observed edge-on and the remaining two planes inclined by an angle of 30°. The existence of several variants of Moire fringes in this figure is magnified in Figure 5c, indicating that the basal planes of hcp precipitates are not perfectly aligned along the <111> planes of the fcc matrix. This phenomenon results from deviations during the transformation process.

To further discern the origin of the diffraction patterns, especially the + shaped diffraction spots, a through-focus dark-field image shifts method ($2\frac{1}{2}$) [45] was employed, as depicted in Figure 6a,b. This method facilitated the sorting and identifying of the four <111> planes when viewed in stereo. Figure 6c presents a typical diffraction pattern associated with partially coherent particles. In hcp precipitates with parallel close-packed planes and directions in an fcc matrix, the precipitate diffraction occurs according to its crystal structure rather than due to matrix distortion. The streaking of the precipitate spots in the diffraction pattern suggests the thin nature of the precipitates, resulting in a complex diffraction pattern. The microstructures and crystal structures of the precipitates align with findings related to γ precipitates in Al-rich Ag-Al alloys, as reported by Moore and Howe [14].

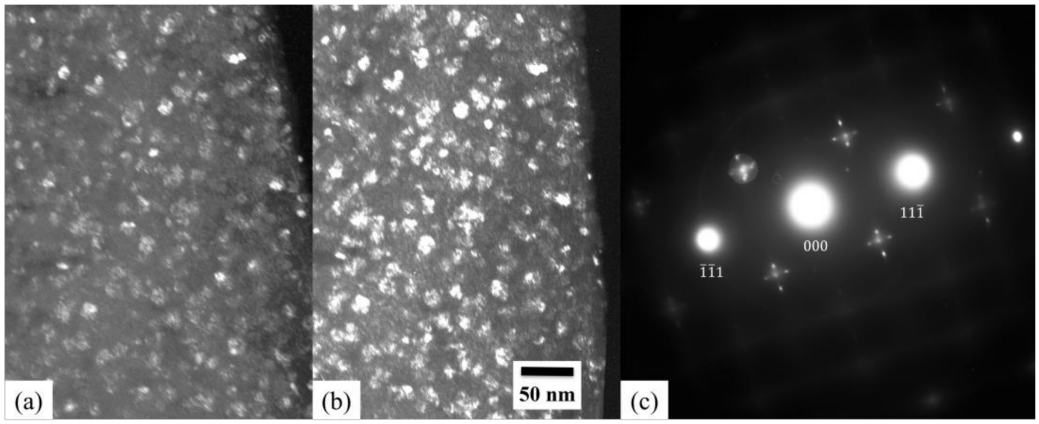


Figure 6. (**a**,**b**) Through-focus dark-field image pairs showing the microstructure of spherical precipitates in Al matrix observed in Al-rich side of the diffusion couple. (**c**) The diffraction pattern of the partially coherent precipitates nearly annealed at 703 K for 70 h.

Various research on precipitation in Al-rich Ag-Al alloys (Howe et al., 1985; Moore & Howe, 2000; Neumann, 1966; Zhang et al., 2019) has shown that the initial microstructural evolution involves a transition from spherical G-P zones to metastable γ' precipitates with stacking faults parallel to the basal plane of the hcp structure. These precipitates subsequently grow into equilibrium γ precipitates through discontinuous precipitation. The exact areas of G-P zones and γ phases within the diffusion couple were confirmed using the FIB technique, which ensures precise localization within the diffusion couple despite introducing FIB-induced damages and heat effects. Figure 6b displays the microstructures of small hcp plate-like phases observed in the specimen prepared using the FIB technique. These precipitates exhibit a growth stage more advanced than that shown in Figure 6a, yet similar diffraction patterns are observed, as depicted in Figure 6c. These patterns reveal a slight deviation from the <100> zone axis, incorporating the zeroth-order Laue zone (ZOLZ) and the first-order Laue zone (FOLZ) of the [100] reciprocal lattice [46]. Satellite spots and diffraction pattern streaking confirm the presence of precipitates formed along the <111> planes within the fcc matrix in platelets, as illustrated in Figure 6c.

3.3. Crystal Structure Analysis of Each Phase

The precise crystal structure, including the ordering and Ag concentration, of the G-P zones and γ precipitates in Ag-Al alloys has been an ongoing debate since their discovery. Numerous research efforts have sought to identify the crystal structure and order of the metastable γ' and the equilibrium γ precipitates in Al-rich Ag-Al alloys. Both precipitates are reported to have a stoichiometric composition of Ag_2Al and exhibit a hcp structure [15]. The metastable γ' precipitates display varying degrees of long-range order (LRO) along the c-axis in the hcp structure. This LRO ranges from a highly ordered arrangement of Ag and Al atoms on alternate basal planes to a disordered arrangement, as demonstrated by previous work by Howe et al. [15]. To align with composition analysis, Howe et al. also proposed another structure characterized by alternating layers, with one plane of 100 at.% Ag and the next layer comprising 33 at.% Ag, particularly relevant in studies of plate-shaped hcp γ precipitates [15].

Conversely, Ag-rich Ag-Al alloys exhibit a bulk equilibrium hcp phase known as the δ phase, accommodating a broad composition range of 23–42 at.% Al [8]. To determine the short-range order (SRO) of the δ phase, the chemical structure of Ag_2Al was studied and proposed by Neumann [19], employing X-ray scattering data. Kitano et al. [47] also investigated the SRO of a disordered δ phase using X-ray and electron diffraction methods. Various simulation techniques were employed to ascertain the stability and ground-state structure of Ag_2Al precipitates [18,48,49]. These studies have indicated that the bulk equilibrium δ phase and γ precipitates share an hcp structure with off-stoichiometric

disordered characteristics but exhibit distinct ordering arrangements within the basal planes of the hcp structure.

In this study, meticulous electron diffraction analysis achieved the clear identification of the crystal structure for each phase. Specifically, regarding the δ phase, distinctive diffraction patterns, emblematic of the hcp structure, were prominently evident. These patterns confirmed the hcp structure and provided compelling evidence of the progressive emergence of well-defined diffraction spots, as visually demonstrated in Figure 4. Similarly, the plate-like γ phase, situated between the δ phase and Al matrix, exhibited an hcp structure accompanied by satellite spots resulting from the precipitates, as depicted in Figure 5b,c. Metastable γ′ precipitates were observed within the Al matrix, taking the form of plates that likely grew from G-P zones.

Notably, Moire fringes were observed on the plate-like precipitates, and these plates exhibited a slight inclination from the fcc {111} planes, as demonstrated in Figure 5. This indicates that the microstructure transforms, transitioning from spherical G-P zones to plate-like shapes along specific {111} planes upon growth [50].

The lattice parameters were meticulously determined from the diffraction patterns. The camera constant, denoted as $2\lambda L_0$, was calculated using the formula:

$$dD = 2\lambda L_0 \tag{3}$$

In this study, the Hitachi H1250S microscope operated at 1020 kV, resulting in a wavelength (λ) of 0.86×10^{-12} m and an effective camera length (L_0) of 1.39 m. The lattice parameters for the δ phase were determined as follows: a = 0.2875 nm and c = 0.4782 nm, with a c/a ratio of 1.6633. It is worth noting that the lattice parameters of the δ phase can vary with the composition of Al. The measured results are consistent with the lattice parameters expected for the δ phase and are in good agreement with Ag-Al lattice parameter data. In contrast, for the γ phase, the lattice parameters were determined to be a = 0.2937 nm and c = 0.4511 nm, resulting in a c/a ratio 1.536. Notably, the length of the c-axis in the γ phase was found to be shorter than that in the δ phase. Within the Al-rich region, the lattice parameter of the Al matrix exhibits a wide range, spanning from a = 0.4087 nm to 0.4158 nm. This variation is consistent with previous findings [16], who reported that the lattice parameters of Al in Ag-Al alloys increase from 0.40496 nm to 0.41057 nm with increasing Ag composition from 0 to 14.6 at.%. The measured lattice parameter of the Al matrix aligns well with the existing literature data and is considered reasonable.

4. Discussion

The observation of an exponent n slightly exceeding 0.5 carries significant implications for understanding the rate-controlling process governing intermetallic layer growth. An n value of 0.5 suggests that the primary factor controlling the growth of the intermediate layer is volume diffusion [51]. This indicates that the movement of atoms within the material is the dominant mechanism influencing the growth process. Conversely, when n equals 1, it implies that interface reactions take precedence in driving layer growth. Interface reactions refer to chemical interactions between different materials at the boundaries or interfaces [34]. Based on the experimental findings, it is evident that volume diffusion predominantly governs the growth of the intermetallic layer. However, it is also clear that interface reactions play a secondary, albeit noteworthy, role in influencing the growth rate. This nuanced understanding sheds light on the underlying mechanisms contributing to the rate-controlling process, providing valuable insights into the interplay between volume diffusion and interface reactions in intermetallic layer growth.

The investigation of phase transformations and the identification of specific phases within alloy systems are essential for understanding material behavior and optimizing material properties. To elucidate the nature of a hitherto unidentified phase located between the δ phase and the Al matrix within the context of a diffusion couple experiment, an Al-25.6Ag alloy was carefully prepared through arc melting and subjected to detailed analysis. The microstructure of the Al-25.6Ag alloy following annealing at 703 K for 641 h was

examined using BEI, as depicted in Figure 2a. Within this micrograph, distinctive features are readily discernible. Bright coarse grains, characterized by their irregular distribution and interconnected configuration, are prominently observed within a darker matrix. This microstructural insight provides an initial understanding of the alloy's composition and structure. Notably, the XRD analysis provides unequivocal evidence of the presence of the stable Ag_2Al phase within the alloy. Additionally, it confirms the coexistence of the Al matrix. These findings are consistent with prior knowledge of the alloy's expected phases. However, the most intriguing aspect of this investigation lies in the identity of the third phase within the equilibrated Al-25.6Ag alloy. Despite the unambiguous confirmation of the Ag_2Al phase and the Al matrix, the nature and characteristics of this unidentified phase remain elusive. This enigmatic phase presents a compelling scientific challenge, as its properties, crystal structure, and role within the alloy system are yet to be determined.

The concentrations of the stable intermediate phases were plotted on the binary Al-Ag phase diagram, as shown in Figure 7. Interestingly, the solubility range of these intermediate phases was shifted and narrower compared to the calculated phase diagram. This shift implies that the behavior of intermediate phases, particularly their formation and stability, does not conform to the theoretical predictions of the phase diagram. This discrepancy raises intriguing questions about the underlying mechanisms that govern the formation of these phases in real-world conditions. The narrower solubility range of the intermediate phases has practical implications. It means that these phases may be more sensitive to changes in temperature and composition than previously thought. This sensitivity could be harnessed for various applications, such as in controlling the microstructure and properties of materials, which is crucial in industries like electronics, where precise control over material properties is essential. Understanding the solubility range of intermediate phases is paramount in materials design and engineering. The narrower solubility range suggests that precise control over these phases is feasible, enabling the development of novel materials with unique characteristics [52].

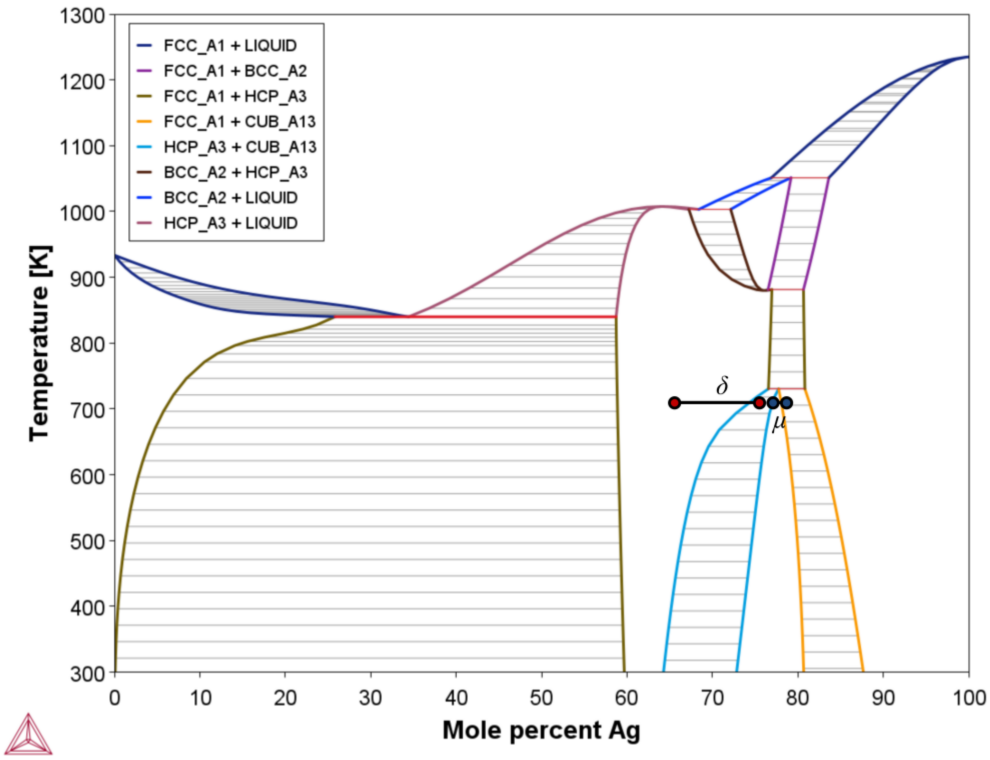


Figure 7. Stable intermediate phases in the present study were plotted using the solid line with color circles on the binary Al-Ag phase diagram calculated by ThermoCalc.

The δ phase exhibits plate-like structures with a refined grain arrangement, confirmed to possess an hcp structure in the [031] and [011] zones. The fine-grained nature occasionally leads to double diffraction, resulting in faint extra spots. In contrast, the intermediate phase between the δ phase and the Al matrix reveals hcp lamellar structures. Diffraction patterns in the [100] zone exhibit streaking perpendicular to the stacking directions, attributed to factors like stacking faults and thin-ordered phases. The intensity of streaking indicates changes in lamellar phase ordering during growth, with similar patterns observed in other materials. On the Al side, near the interface between the intermediate phase and the Al matrix, plate-like precipitates are observed. These are identified as plate-like hcp phases along the <111> planes within the Al matrix. The transformation from initial spherical nano-sized G-P zones to plate-like structures is discussed, emphasizing growth and alignment along specific planes [53]. Using experimental techniques like the FIB method enhances the credibility of these observations. Overall, this analysis of each layer in the diffusion couple enhances our understanding of microstructural changes and phase transformations within the Ag/Al diffusion couple, setting the stage for further analysis and discussion.

Microstructure evolution at the interface of the diffusion couple is a complex and dynamic process driven by diffusion, phase transformations, and the interaction between different materials. In the case of the Ag/Al diffusion couple, several key stages in microstructural evolution can be identified. At the onset of the diffusion experiment, there is a well-defined interface between the Ag and Al materials. This initial interface is typically smooth and devoid of any intermediate phases or microstructural changes. As the diffusion process begins, Ag atoms migrate into the Al matrix, forming an intermediate phase known as the δ phase. This phase appears as plate-like structures with refined grains. Electron diffraction patterns reveal that the δ phase adopts a hcp structure. The region between the δ phase and the Al matrix undergoes significant changes. It features hcp lamellar structures, indicating the presence of a different phase or microstructure. Diffraction patterns in this area exhibit streaking, which is attributed to various factors, such as stacking faults and thin-ordered phases. The intensity of streaking provides insights into changes in the ordering of the lamellar phase during growth. On the Al side of the interface, closer to the Al matrix, plate-like precipitates become evident. These precipitates are identified as plate-like hcp phases and are aligned along specific <111> planes within the Al matrix. The growth of these precipitates involves the transformation of initially spherical nano-sized G-P zones into plate-like structures. The G-P zones likely serve as nucleation sites for the plate-like precipitates. The microstructural evolution at the interface is a function of both time and temperature. Prolonged annealing at elevated temperatures allows for further growth and development of these intermediate phases. The microstructural changes observed over time provide valuable insights into the kinetics of phase transformations and diffusion processes. Advanced techniques, such as FIB methods, are employed to characterize these microstructural changes precisely. These techniques ensure accurate specimen preparation and localization within the diffusion couple despite potential FIB-induced damages and heat effects [54]. In summary, the evolution of microstructure at the interface of the Ag/Al diffusion couple involves the formation of intermediate phases (e.g., δ phase and plate-like precipitates), changes in grain structure, and diffraction pattern variations. These observations provide a detailed understanding of the complex interplay of diffusion, phase transformations, and microstructural changes at the interface. This is essential for comprehending the behavior of such diffusion couples in various applications and materials systems.

Figure 8 illustrates a schematic diagram detailing the evolution of precipitates and phase growth resulting from reactive diffusion. It is assumed that Ag atoms initially form spherical G-P zones within the Al matrix during diffusion in the Al side of the Ag/Al diffusion couple. As the influx of Ag atoms progresses, it is hypothesized that these G-P zones undergo growth, transforming into γ' plates. Concurrently, the diffusion process is expected to induce the formation of Ag-rich stacking faults and metastable γ' precipitates within the Al matrix, as demonstrated in Figure 5a. Subsequently, plate-like γ precipitates

emerge through the further growth of the initially formed γ' precipitates. This growth occurs along the basal plane of the hcp phase, giving rise to a lamellar structure oriented along the {111} planes of Al. As a result, the intermediate phase identified by EPMA between the δ phase and Al matrix can be attributed to the coexistence of the equilibrium γ phase, characterized by its hcp lamellar structure, and the precipitation of γ' phase. The outcomes of successive observations, from the Al matrix to the δ phase, align with the growth characteristics of γ precipitates observed in Ag-Al alloys, as reported in prior studies [14,19]. These investigations collectively point to a growth process involving heterogeneous and homogeneous mechanisms within the mutual diffusion couple.

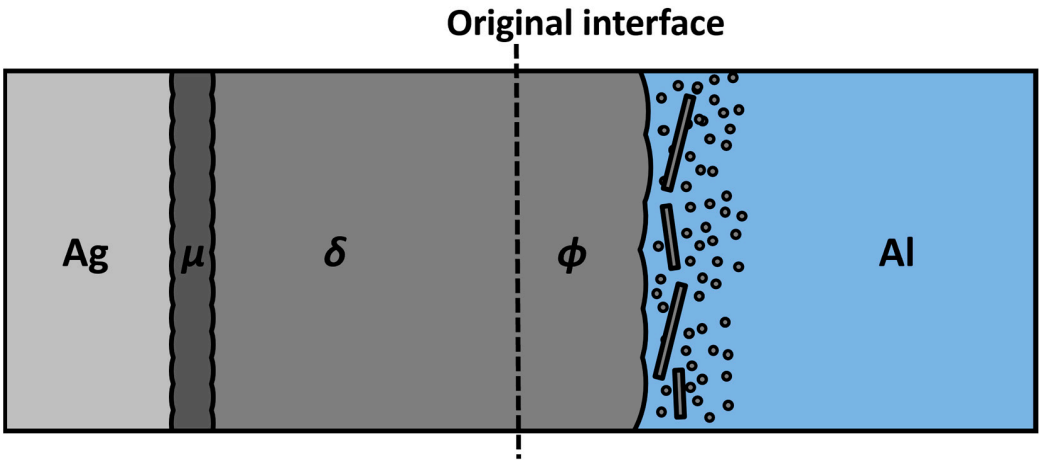


Figure 8. Illustration depicting the microstructure evolution and phase transformation at the interface.

This study could impact the electronic component design field significantly. Delving into the behavior and properties of intermediate phases within the Ag-Al system opens the door to developing novel materials with precisely tailored properties [55]. This knowledge promises to create electronic components that exhibit superior performance, increased durability, and enhanced reliability. Furthermore, the insights garnered from this research can revolutionize manufacturing processes for electronic components. The ability to control the growth and characteristics of intermediate phases provides manufacturers with the means to produce components that function with enhanced capabilities and exhibit reduced defects. In addition to benefiting manufacturers, electronic component designers and engineers can benefit from a broader array of materials. The findings from this study expand our understanding of the Ag-Al system, introducing fresh possibilities for material selection in the realm of electronic device fabrication. The fine-tuning of material properties, which this research facilitates, directly influences the performance of electronic devices. With these newfound insights, designers can craft components that offer superior conductivity, improved thermal characteristics, and heightened resistance to corrosion. In essence, this study has the potential to drive the development of electronic components that are more reliable and durable and deliver enhanced performance. Such advancements will ultimately redound to benefit the entire electronic device industry.

5. Conclusions

In conclusion, this research utilized high-voltage electron microscopy (HVEM) to investigate the dynamic evolution of microstructures and the growth of intermediate phases within Ag/Al diffusion couples. Comprehensive observations of various regions within these diffusion couples provided valuable insights. The δ phase was identified as having a plate-like lamellar structure characterized by a fine-grained internal composition. Similarly, the intermediate phase between the δ phase and the Al matrix exhibited a hexagonal close-packed (hcp) lamellar structure. Plate-like precipitates were observed near the boundary between the intermediate phase and the Al matrix. These nano-sized precipitates, believed to originate as spherical Guinier–Preston (G-P) zones within the

Al matrix, transformed into plate-like structures as they grew along specific {111} planes during diffusion. Furthermore, electron diffraction techniques were employed to determine the crystal structures and lattice parameters of each phase, and the results consistently align with prior research findings. Key discoveries from this study include the plate-like lamellar structure of the δ phase, the hcp lamellar structure in the intermediate phase, and the transformation of nano-sized G-P zones into plate-like precipitates. This study clearly explained the evolutionary processes and growth mechanisms of Al-rich intermediate phases within Ag/Al diffusion couples. The proposed sequence suggests that transferred Ag atoms initially manifest as spherical G-P zones within the Al matrix. Over time, these G-P zones mature into metastable γ' precipitates. Simultaneously, the heterogeneous formation of γ' precipitates occurs along stacking faults within the Al matrix, resulting in the development of an hcp lamellar structure along the {111} planes of Al. Consequently, this research identifies the progression from off-stoichiometric disordered intermediate phases to ordered phases at the interface of Ag/Al diffusion couples. This study holds significant promise in the field of electronic component design. Exploring intermediate phases in the Ag-Al system paves the way for developing customized materials, leading to electronic components with enhanced performance and durability. It also offers potential advancements in manufacturing processes, allowing for better control of component characteristics and reduced defects. These findings expand the range of materials available to designers, resulting in electronic components with superior conductivity, thermal properties, and corrosion resistance. Ultimately, this research has the potential to yield more reliable and high-performance components, benefitting the electronic device industry.

Author Contributions: Conceptualization, M.O. and M.K.; methodology, M.O.; software, M.O.; validation, M.O. and M.K.; formal analysis, M.O.; investigation, M.O.; writing—original draft preparation, M.O.; visualization, M.O.; supervision, M.K. All authors have read and agreed to the published version of the manuscript.

Funding: This research received the external funding from the Iketani Science and Technology Foundation (0351095-A, Tokyo Japan), and the Light Metals Educational Foundation, Inc. (Osaka Japan).

Data Availability Statement: The data presented in this study are available upon request from the corresponding author.

Acknowledgments: M.O. and M.K. thank A. Sato of the Tokyo Institute of Technology for providing invaluable support and engaging in insightful discussions during the HVEM observation.

Conflicts of Interest: The authors declare no conflict of interest.

References

1. Fu, S.W.; Lee, C.C. A Study on Intermetallic Compound Formation in Ag–Al System and Evaluation of Its Mechanical Properties by Micro-Indentation. *J. Mater. Sci. Mater. Electron.* **2018**, *29*, 3985–3991. [CrossRef]
2. Chang, L.P.; Huang, S.Y.; Chang, T.C.; Ouyang, F.Y. Low Temperature Ag-Ag Direct Bonding under Air Atmosphere. *J. Alloys Compd.* **2021**, *862*, 158587. [CrossRef]
3. Alderete, B.; Mücklich, F.; Suarez, S. Tarnishing (Ag2S) Layer on Silver-Plated Electrical Contacts: Its Influence on Electrical Contact Resistance. *IEEE Trans. Compon. Packag. Manuf. Technol.* **2023**, *13*, 45–58. [CrossRef]
4. Meguro, K.; O, M.; Kajihara, M. Growth Behavior of Compounds Due to Solid-State Reactive Diffusion between Cu and Al. *J. Mater. Sci.* **2012**, *47*, 4955–4964. [CrossRef]
5. O, M.; Kajihara, M. Kinetics of Solid-State Reactive Diffusion between Au and Al. *Mater. Trans.* **2011**, *52*, 677–684. [CrossRef]
6. Odashima, N.; O, M.; Kajihara, M. Formation of Intermetallic Compounds and Microstructure Evolution Due to Isothermal Reactive Diffusion at the Interface Between Solid Co and Liquid Sn. *J. Electron. Mater.* **2020**, *49*, 1568–1576. [CrossRef]
7. Zarkevich, N.A.; Johnson, D.D. Predicted Hcp Ag-Al Metastable Phase Diagram, Equilibrium Ground States, and Precipitate Structure. *Phys. Rev. B Condens. Matter Mater. Phys.* **2003**, *67*, 064104. [CrossRef]
8. McAlister, A.J. The Ag-Al (Silver-Aluminum) System. *Bull. Alloy Phase Diagr.* **1987**, *8*, 526–533. [CrossRef]
9. Ben, F.; Olubambi, P.A. Phase and Properties Prediction of Al–Ag Binary System Using Thermo-Calc. *MRS Adv.* **2023**, 1–6. [CrossRef]
10. Fouracre, R.A. Electron Microscope Observations and Measurements in the Al/Ag Thin Film System. *Thin Solid Film.* **1987**, *146*, 83–92. [CrossRef]

11. Roy, R.; Sen, S.K. Calorimetric and Other Studies of Intermetallic Phase Formation in Ag/Al Bilayer Thin Films. *J. Mater. Sci.* **1992**, *27*, 6098–6104. [CrossRef]
12. Schleiwies, J.; Schmitz, G. Thin Film Interreaction of Al/Ag Analyzed by Tomographic Atom Probe. *Mater. Sci. Eng. A* **2002**, *327*, 94–100. [CrossRef]
13. Pang, M.; Zhan, Y.; Yang, W.; Li, C.; Wang, H.; Jiang, W.; Du, Y. First-Principles Calculations on the Crystal, Electronic Structures and Elastic Properties of Ag-Rich Γ′ Phase Approximates in Al-Ag Alloys. *Comput. Mater. Sci.* **2012**, *51*, 415–421. [CrossRef]
14. Moore, K.T.; Howe, J.M. Characterization of γ Plate-Shaped Precipitates in an Al-4.2 at.% Ag Alloy-Growth Kinetics, Solute Field, Composition and Modeling. *Acta Mater.* **2000**, *48*, 4083–4098. [CrossRef]
15. Howe, J.M.; Aaronson, H.I.; Gronsky, R. Atomic Mechanisms of Precipitate Plate Growth in the AlAg System-II. High-Resolution Transmission Electron Microscopy. *Acta Metall.* **1985**, *33*, 649–658. [CrossRef]
16. Zhang, Z.; Rosalie, J.M.; Medhekar, N.V.; Bourgeois, L. Resolving the FCC/HCP Interfaces of the γ′ (Ag2Al) Precipitate Phase in Aluminium. *Acta Mater.* **2019**, *174*, 116–130. [CrossRef]
17. Nicholson, R.B.; Nutting, J. The Metallography of Precipitation in an Al-16% Ag Alloy. *Acta Metall.* **1961**, *9*, 332–343. [CrossRef]
18. Zarkevich, N.A.; Johnson, D.D.; Smirnov, A.V. Structure and Stability of Hcp Bulk and Nano-Precipitated Ag2Al. In *Acta Materialia*; Elsevier: Amsterdam, The Netherlands, 2002; Volume 50.
19. Neumann, J.P. Determination of the Ordering in the Intermetallic Compound Ag2Al. *Acta Metall.* **1966**, *14*, 505–511. [CrossRef]
20. Takamatsu, Y.; O, M.; Kajihara, M. Kinetics of Reactive Diffusion in the Co/Zn System at Solid-State Temperatures. *Mater. Trans.* **2017**, *58*, 567–573. [CrossRef]
21. Nakayama, M.; O, M.; Kajihara, M. Experimental Observation of Diffusion Reaction in the (Sn-Ag)/Cu System at Solid-State Temperatures. *J. Electron. Mater.* **2019**, *48*, 1766. [CrossRef]
22. O, M.; Tanaka, Y.; Kobayashi, E. Microstructure Evolution at the Interface between Cu and Eutectic Sn-Bi Alloy with the Addition of Ag or Ni. *J. Mater. Res. Technol.* **2023**, *26*, 8165–8180. [CrossRef]
23. O, M.; Tanaka, Y.; Kobayashi, E. Growth Behavior of Intermetallic Layers at the Interface between Cu and Eutectic Sn–Bi by Grain Boundary Diffusion with the Grain Growth at Solid-State Temperatures. *Intermetallics* **2023**, *161*, 107986. [CrossRef]
24. Inada, H.; Kakibayashi, H.; Isakozawa, S.; Hashimoto, T.; Yaguchi, T.; Nakamura, K. Hitachi's Development of Cold-Field Emission Scanning Transmission Electron Microscopes. *Adv. Imaging Electron Phys.* **2009**, *159*, 123–186.
25. Matsumoto, S.; Sato, A.; Mori, T. Formation of h.c.p. and f.c.c. Twins in an FeMnCrSiNi Alloy. *Acta Metall. Mater.* **1994**, *42*, 1207–1213. [CrossRef]
26. Li, J.; Malis, T.; Dionne, S. Recent Advances in FIB-TEM Specimen Preparation Techniques. *Mater. Charact.* **2006**, *57*, 64–70. [CrossRef]
27. Michalcová, A.; Marek, I.; Knaislová, A.; Sofer, Z.; Vojtěch, D. Phase Transformation Induced Self-Healing Behavior of Al-Ag Alloy. *Materials* **2018**, *11*, 199. [CrossRef] [PubMed]
28. O, M.; Vakanas, G.; Moelans, N.; Kajihara, M.; Zhang, W. Formation of Compounds and Kirkendall Vacancy in the Cu-Sn System. *Microelectron. Eng.* **2014**, *120*, 133–137. [CrossRef]
29. Vakanas, G.; O, M.; Dimcic, B.; Vanstreels, K.; Vandecasteele, B.; De Preter, I.; Derakhshandeh, J.; Rebibis, K.; Kajihara, M.; De Wolf, I.; et al. Formation, Processing and Characterization of Co-Sn Intermetallic Compounds for Potential Integration in 3D Interconnects. *Microelectron. Eng.* **2015**, *140*, 72–80. [CrossRef]
30. O, M.; Suzuki, T.; Kajihara, M. Kinetics of Isothermal Reactive Diffusion Between Solid Cu and Liquid Sn. *J. Electron. Mater.* **2018**, *47*, 18–26. [CrossRef]
31. Murakami, S.; O, M.; Kajihara, M. Growth Behavior of Compounds during Reactive Diffusion in the Solid-Cu/Liquid-Sn System. *Mater. Trans.* **2018**, *59*, 198–203. [CrossRef]
32. Kizaki, T.; O, M.; Kajihara, M. Rate-Controlling Process of Compound Growth in Cu-Clad Al Wire during Isothermal Annealing at 483-543K. *Mater. Trans.* **2020**, *61*, 188–194. [CrossRef]
33. Atkinson, H.V. Overview No. 65. Theories of Normal Grain Growth in Pure Single Phase Systems. *Acta Metall.* **1988**, *36*, 469–491. [CrossRef]
34. O, M.; Sato, K.; Kobayashi, E. Investigation of the Rate-Controlling Process of Intermetallic Layer Growth at the Interface between Ferrous Metal and Molten Al–Mg–Si Alloy. *Intermetallics* **2023**, *163*, 108069. [CrossRef]
35. Haerifar, M.; Azizian, S. Mixed Surface Reaction and Diffusion-Controlled Kinetic Model for Adsorption at the Solid/Solution Interface. *J. Phys. Chem. C* **2013**, *117*, 8310–8317. [CrossRef]
36. Sun, W. Kinetics for Coarsening Co-Controlled by Diffusion and a Reversible Interface Reaction. *Acta Mater.* **2007**, *55*, 313–320. [CrossRef]
37. O, M.; Takamatsu, Y.; Kajihara, M. Kinetics of Solid-State Reactive Diffusion between Co and Sn. *Mater. Trans.* **2014**, *55*, 1058–1064. [CrossRef]
38. Chen, W.H.; Yu, C.F.; Cheng, H.C.; Tsai, Y.M.; Lu, S.T. IMC Growth Reaction and Its Effects on Solder Joint Thermal Cycling Reliability of 3D Chip Stacking Packaging. *Microelectron. Reliab.* **2013**, *53*, 30–40. [CrossRef]
39. Jiao, L.; Seow, J.Y.R.; Skinner, W.S.; Wang, Z.U.; Jiang, H.L. Metal–Organic Frameworks: Structures and Functional Applications. *Mater. Today* **2019**, *27*, 43–68. [CrossRef]
40. Su, R.; Neffati, D.; Zhang, Y.; Cho, J.; Li, J.; Wang, H.; Kulkarni, Y.; Zhang, X. The Influence of Stacking Faults on Mechanical Behavior of Advanced Materials. *Mater. Sci. Eng. A* **2021**, *803*, 140696. [CrossRef]

41. Jomni, S.; Mliki, N.; Belhi, R.; Abdelmoula, K.; Ayadi, M.; Nihoul, G. Face Centered Cubic Cobalt Ultrathin-Layers in Au/Co(111) Multilayers: A Study by Electron Diffraction and by HREM. *Thin Solid Film.* **2000**, *370*, 186–191. [CrossRef]
42. Chen, X.; O, M.; Kobayashi, E. Enhanced Mechanical Properties in an Al-Mg-Cu Alloy Processed by the Combination of Cyclic Deformation and Aging Heat Treatment. *J. Alloy. Compd.* **2022**, *911*, 165070. [CrossRef]
43. Kirekawa, N.; Saito, K.; O, M.; Kobayashi, E. Effect of Cold Rolling on Cluster(1) Dissolvability during Artificial Aging and Formability during Natural Aging in Al-0.6Mg-1.0Si-0.5Cu Alloy. *Metals* **2022**, *12*, 92. [CrossRef]
44. Chen, X.; Mørtsell, E.A.; Sunde, J.K.; O, M.; Marioara, C.D.; Holmestad, R.; Kobayashi, E. Enhanced Mechanical Properties in 6082 Aluminum Alloy Processed by Cyclic Deformation. *Metals* **2021**, *11*, 1735. [CrossRef]
45. Bell, W.L. 2 1/2D Electron Microscopy: Through-Focus Dark-Field Image Shifts. *J. Appl. Phys.* **1976**, *47*, 1676–1682. [CrossRef]
46. Zuo, J.M.; Spence, J.C.H. The Geometry of Electron Diffraction Patterns. In *Advanced Transmission Electron Microscopy*; Springer: Berlin/Heidelberg, Germany, 2017.
47. Kitano, Y.; Komura, Y.; Fujiwara, K.; Iio, A. Short Range Order Diffuse Scattering from Disordered ζ Phase, Ag-Al. *J. Phys. Soc. Jpn.* **1976**, *40*, 593–594. [CrossRef]
48. Peng, M.; Zhao, Y.; Lan, J.; Qiao, Y.; Tan, Y. Self-Standing 3D Nanoporous Ag2Al with Abundant Surface Oxygen Species Facilitating Oxygen Electroreduction for Efficient Hybrid Zn Battery. *J. Energy Chem.* **2021**, *58*, 345–354. [CrossRef]
49. Tian, S.; Liu, Y.; Ma, Q.; Zhang, P.; Zhou, J.; Xue, F.; Sun, Z.M. Intermetallics-Induced Directional Growth of Sn Whiskers in Sn-3.5Ag Coating on Al Substrate. *Appl. Surf. Sci.* **2021**, *539*, 148135. [CrossRef]
50. Liu, C.; Yuan, F.; Han, F.; Ali, M.; Zhang, Y.; Guo, W.; Gu, H.; Li, G. Moiré Fringes in Nanoprecipitates in a Zirconium Alloy. *Mater. Lett.* **2020**, *269*, 127678. [CrossRef]
51. O, M.; Fujita, H.; Kobayashi, E.; Kajihara, M. Kinetics and Thermodynamics of Compound Growth Due to Reactive Diffusion between Solid Cu and Binary Bi-Sn Alloys. *J. Mol. Liq.* **2022**, *348*, 118063. [CrossRef]
52. Cowan, M.J.; Higaki, T.; Jin, R.; Mpourmpakis, G. Understanding the Solubility Behavior of Atomically Precise Gold Nanoclusters. *J. Phys. Chem. C* **2019**, *123*, 20006–20012. [CrossRef]
53. Thanh, N.T.K.; Maclean, N.; Mahiddine, S. Mechanisms of Nucleation and Growth of Nanoparticles in Solution. *Chem. Rev.* **2014**, *114*, 7610–7630. [CrossRef] [PubMed]
54. Kodentsov, A.; Paul, A. Diffusion Couple Technique: A Research Tool in Materials Science. In *Handbook of Solid State Diffusion*; Elsevier: Amsterdam, The Netherlands, 2017; Volume 2.
55. Manjunatheshwara, K.J.; Vinodh, S. Sustainable Electronics Product Design and Manufacturing: State of Art Review. *Int. J. Sustain. Eng.* **2021**, *14*, 541–551. [CrossRef]

Disclaimer/Publisher's Note: The statements, opinions and data contained in all publications are solely those of the individual author(s) and contributor(s) and not of MDPI and/or the editor(s). MDPI and/or the editor(s) disclaim responsibility for any injury to people or property resulting from any ideas, methods, instructions or products referred to in the content.